analytical chemistry

Article

pubs.acs.org/ac

In Situ Generation of Electron Acceptor for Photoelectrochemical Biosensing via Hemin-Mediated Catalytic Reaction

Yang Zang, Jianping Lei,* Lei Zhang, and Huangxian Ju

State Key Laboratory of Analytical Chemistry for Life Science, School of Chemistry and Chemical Engineering, Nanjing University, Nanjing 210093, People's Republic of China

ABSTRACT: A novel photoelectrochemical sensing strategy is designed for DNA detection on the basis of in situ generation of an electron acceptor via the catalytic reaction of hemin toward H_2O_2. The photoelectrochemical platform was established by sequential assembly of near-infrared CdTe quantum dots, capture DNA, and a hemin-labeled DNA probe to form a triple-helix molecular beacon (THMB) structure on an indium tin oxide electrode. According to the highly catalytic capacity of hemin toward H_2O_2, a photoelectrochemical mechanism was then proposed, in which the electron acceptor of O_2 was in situ-generated on the electrode surface, leading to the enhancement of the photocurrent response. The utilization of CdTe QDs can extend the absorption edge to the near-infrared band, resulting in an increase in the light-to-electricity efficiency. After introducing target DNA, the THMB structure is disassembled and releases hemin and, thus, quenches the photocurrent. Under optimized conditions, this biosensor shows high sensitivity with a linear range from 1 to 1000 pM and detection limit of 0.8 pM. Moreover, it exhibits good performance of excellent selectivity, high stability, and acceptable fabrication reproducibility. This present strategy opens an alternative avenue for photoelectrochemical signal transduction and expands the applications of hemin-based materials in photoelectrochemical biosensing and clinical diagnosis.

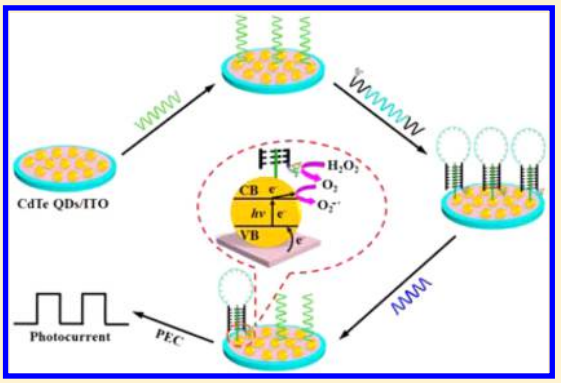

DNA sensors are of crucial importance to the determination of many biological markers of disease and have been extensively applied in many areas, such as clinical diagnosis, pathogen detection, and gene therapy.[1−3] Several DNA structures have been involved in DNA sensing, such as the triple-helix molecular beacon (THMB),[4] G-quadruplex[5] and other DNA conformations.[6,7] Interestingly, THMB, consisting of a hairpin-shaped DNA probe flanked by two arm segments and a single-strand DNA,[8] can be easily used to develop a DNA biosensor owing to its detachable stem−loop structure, excellent molecular recognition properties, and desirable selectivity. On the other hand, various analytical techniques have been used for DNA detection, including fluorescence,[9] colorimetry,[10] electrochemistry,[11] photoelectrochemistry (PEC),[12] and electrochemiluminescence.[13] Among them, the photoelectrochemical technique has received substantial attention because of its desirable background signal and low applied potential.[14−17] The conventional strategies of PEC often rely on steric hindrance during biorecognition events,[18] resonance energy transfer,[19] and consumption/generation of coreactant.[20,21] Significantly, the consumption/generation of coreactant through electrocatalysis or enzymatic reaction is one primary methodology in the construction of a photoelectrochemical sensing strategy.

Recently, several enzyme-based photoelectrochemical strategies have been designed for bioassays.[22,23] For example, on the basis of the consumption of O_2 by catalytic reaction of glucose oxidase, a light-controlled photoelectrochemical sensor was constructed to detect enzymatic activity of glucose oxidase.[24] A sensitive photoelectrochemical immunoassay based on enzymatic ascorbic acid production as an electron donor was used for the determination of prostate-specific antigen with a detection limit of 0.5 ng mL^{-1}.[25] However, the assembly of natural enzyme onto the DNA-sensing platform requires complicated operation because of its relatively larger occupied volume. Moreover, the catalytic property of the natural enzyme strictly relies on its conformation and specific substrate.[26] Thus, searching for a mimic of enzyme with a high catalytic activity, simple operation, and effective immobilization capability is necessary and desirable in practice.

Fe(III)-protoporphyrin IX (hemin) as the catalytic center of peroxidase, myoglobin, and hemoglobin has attracted extensive attention in biomimetic catalysis of simulated enzymes;[27−29] however, direct application of hemin as a mimic catalyst is a significant challenge because of its molecular aggregation in aqueous solution, leading to the passivation of its catalytic activity.[30] An alternative solution to this problem is designed by the assembly of hemin with DNA, graphene, or carbon nanotube. For instance, when covalent binding to oligonucleotides without the requirement of specific sequences, hemin demonstrates a high catalytic property owing to good water solubility and few inactive dimers.[31] By coupling hemin with a

Received: October 6, 2014
Accepted: November 13, 2014
Published: November 13, 2014

   dx.doi.org/10.1021/ac503741x | *Anal. Chem.* 2014, 86, 12362−12368

Scheme 1. Schematic Illustration of Stepwise Construction of the CdTe/Hemin-Labeled THMB Sensing Platform and Photoelectrochemical Strategy for Sensitive Detection of DNA via the Hemin-Mediated Catalytic Reaction

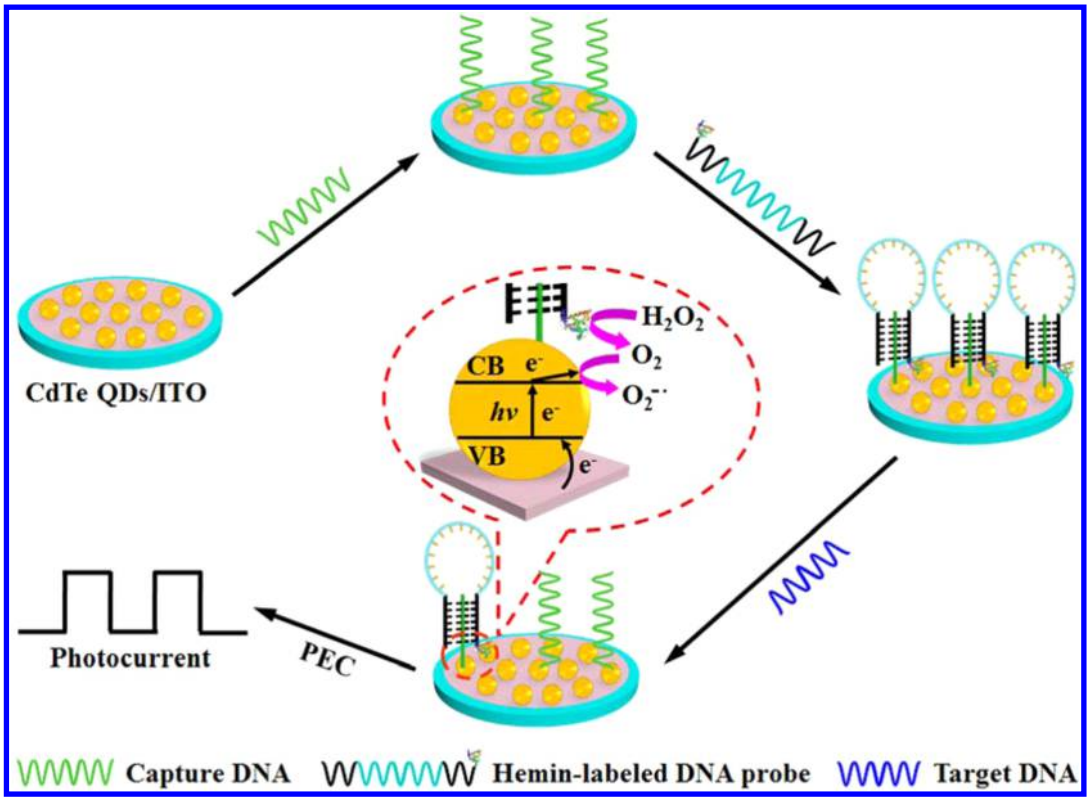

G-quadruplex, the catalytic activity of the hemin/G-quadruplex DNAzyme toward H_2O_2 can be greatly enhanced compared with free hemin.[32,33] Moreover, hemin has been identified as a catalyst for in situ generation of O_2 through the decomposition of H_2O_2.[34,35] These functions can be implemented to design various bioassay methods by using hemin-labeled DNA as a signal tag.

In this work, by integrating near-infrared CdTe QDs, hemin-mediated catalytic reaction and THMB structure switching, a sensitive and selective photoelectrochemical biosensor is developed for DNA detection (Scheme 1). The photoelectrochemical sensing platform is constructed via stepwise modification of CdTe QDs, capture DNA (C-DNA), and hemin-labeled DNA probe (HLDP). The HLDP has a central, target-specific DNA sequence and two arm segments labeled with hemin at the 5′ terminus. When C-DNA serves as the capture module for HLDP binding event to form THMB structure, hemin can be introduced to the electrode surface, which can catalyze H_2O_2 to in situ generate an amount of O_2 as an electron acceptor, leading to the enhancement of the photocurrent signal. In the presence of target DNA, THMB disassembles and releases hemin, which can significantly decrease the photoelectrochemical response owing to the lower catalytic production of O_2. Therefore, on the basis of the THMB structure switching and in situ generation of O_2 as the electron acceptor, a photoelectrochemical biosensor with high sensitivity and excellent selectivity is achieved for the detection of DNA and provides a new concept for photoelectrochemical signal transduction.

EXPERIMENTAL SECTION

Materials and Reagents. The indium tin oxide (ITO) electrode was purchased from Zhuhai Kaivo Electronic Components Co. Ltd. (China). Mercaptopropionic acid (MPA), *n*-hydroxysuccinimide (NHS), 1-ethyl-3-(3-(dimethylamino)propyl)carbodiimide (EDC), and monoethanolamine (MEA) were obtained from Sigma-Aldrich. Cadmium chloride ($CdCl_2$) was purchased from Alfa Aesar China Ltd. Sodium borohydride was purchased from Tianjin Chemagent Research Co. Ltd. All the other chemicals were of analytical grade and were used without further purification. All aqueous solutions were prepared using ultrapure water obtained from a Millipore water purification system (≥18 MΩ, Milli-Q, Millipore). All oligonucleotides used in this study were obtained from Sangon Biotechnology Co. Ltd. (Shanghai, China) and dissolved in 10 mM phosphate buffered saline (PBS) of pH 5.3 containing 20 mM NaCl and 2.5 mM $MgCl_2$. The corresponding sequences are summarized below:

C-DNA: 5′-NH_2-AAAAGGAGAGAG-3′

HLDP: 5′-hemin-CCTCTCTCATGTGGAAAATCTC-TAGCAGTCTCTCTCC-3′

Dual-labeled DNA probe: 5′-Cy3-CCTCTCTCATGTG-GAAAATCTCTAGCAGTCTCT CTCC-BHQ2-3′

Label-free DNA probe: 5′-CCTCTCTCATGTG-GAAAATCTCTAGCAGTCTCTCTCC-3′

Target DNA: 5′-ACTGCTAGAGATTTTCCACAT-3′

Single-base mismatched DNA (smDNA): 5′-ACTGCTA-GAGAGTTTCCACAT-3′

Three-base mismatched DNA (tmDNA): 5′-ACTGTTAGA-GAGTTTCAACAT-3′

Apparatus. The transmission electron micrograph (TEM) image was acquired using a JEM-2100 instrument (JEOL,

dx.doi.org/10.1021/ac503741x | *Anal. Chem.* 2014, 86, 12362−12368

Japan). Fluorescence measurements were conducted on a RF-5301PC fluorescence spectrometer (Shimadzu Co., Japan) equipped with a xenon lamp. UV−vis absorption spectra were obtained using a UV-3600 UV−vis−NIR spectrophotometer (Shimadzu Co. Kyoto, Japan). Dynamic light scattering (DLS) measurements were performed by a BI-200 SM light scattering apparatus (Brookhaven Instruments Co., USA) equipped with a digital correlator at 640 nm. The circular dichroism (CD) spectra were acquired on a JASCO J-810−150S circular spectropolarimeter (Tokyo, Japan), of which the lamp was always kept under a stable stream of dry purified nitrogen (99.99%) during experiments. The X-ray photoelectron spectrum (XPS) was recorded on an ESCALAB 250 spectrometer (Thermo-VG Scientic Co. USA) with an ultrahigh vacuum generator. The photoelectrochemical detections were performed on a Zahner workstation (Zahner, German) with a LW505 light as the accessory light source. Electrochemical impedance spectroscopy (EIS) was obtained on a PGSTAT30/FRA2 system (Autolab, The Netherlands) in 0.1 M Na_2SO_4 solution containing 5 mM of a $K_4[Fe(CN)_6]$/$K_3[Fe(CN)_6]$ (1:1) mixture as the redox probe from 0.1 Hz to 100 kHz with a signal amplitude of 5 mV. Cyclic voltammetry (CV) measurements were performed on a CHI 630D electrochemical workstation (CH Instruments Inc. USA). All electrochemical and photoelectrochemical experiments were carried out at room temperature using a conventional three-electrode system with a modified ITO (4 mm in diameter) or glassy carbon electrode (4 mm in diameter) as working, a platinum electrode as auxiliary, and a saturated calomel as reference electrodes.

Synthesis of MPA-Capped CdTe QDs. CdTe QDs were synthesized by using a slightly modified procedure.[36] Briefly, 0.37 mM of $CdCl_2$ and 0.94 mM of MPA were added to 135 mL of deionized water with N_2 bubbled for 30 min. During this time, the mixture solution was adjusted to pH 9.0 with 1.0 M NaOH, then the freshly prepared NaHTe solution was injected under stirring. The typical molar ratio of Cd^{2+}/NaHTe/MPA was 4:1:10. The resulting mixture solution was subsequently heated to 110 °C and refluxed for some time to obtain the QDs. Before usage, the solution of QDs was precipitated with an equivalent amount of ethanol and collected by centrifugation. The colloidal precipitate was then dissolved in ultrapure water and stored at 4 °C in the dark for subsequent experiments.

Fabrication of Photoelectrochemical Sensing Platform. The ITO slices were cut into 4.7 cm × 1 cm pieces, sonicated in 1.0 M NaOH, 10% H_2O_2, and acetone, followed by cleaning with deionized water thoroughly, and blow-dried with nitrogen prior to use. The CdTe/hemin-labeled THMB modified ITO electrode was prepared as follows: First, 10 μL of CdTe QDs was applied to the electrode and dried at room temperature. Then the modified electrode was activated in 20 μL of 10 mM PBS of pH 5.3 containing 10 mM EDC and 20 mM NHS for 1 h at room temperature. Subsequently, 20 μL of 1 μM C-DNA was applied to the electrode surface and incubated at 4 °C overnight for the covalent coupling between the −COOH group of QDs and the $-NH_2$ group of the DNA. After being blocked with 1 mM MEA, a triple-helix conformation was generated by incubation with 20 μL of 1.0 μM HLDP for 2 h. The electrode was washed three times with PBS and blow-dried with nitrogen after each step of the modification process.

Gel Electrophoresis. A 10% native polyacrylamide gel electrophoresis (PAGE) was prepared by using 1× Tris-borate-EDTA (TBE) buffer. The loading sample was mixed with 7 μL of the DNA sample, 1.5 μL of 6× loading buffer, and 1.5 μL of UltraPowerTM dye and kept for 3 min so that the dye could integrate with the DNA completely. To obtain clear photography, the short-sequence C-DNA was labeled with 6-FAM prior to PAGE, The gel electrophoresis was run at 90 V for 90 min in 1× TBE buffer. The resulting board was illuminated with UV light and photographed with a Molecular Imager Gel Doc XR (Bio-Rad, USA).

Photoelectrochemical Detection of DNA. To evaluate the detection performance of the photoelectrochemical biosensor, 20 μL of the target DNA at different concentrations was added onto the modified electrode surface and incubated for 1 h at room temperature. Then the modified electrode was washed with PBS and dried under a N_2 atmosphere. Finally, the biosensor was placed in 0.1 M N_2-saturated PBS of pH 7.4 containing 1.0 mM H_2O_2 for photoelectrochemical detection with light excitation of 505 nm at the applied potential of −0.10 V.

RESULTS AND DISCUSSION

Characterization of CdTe QDs. The CdTe QDs synthesized by the hydrothermal method showed a clear UV−vis absorption at 638 nm (Figure 1A, curve a), indicating

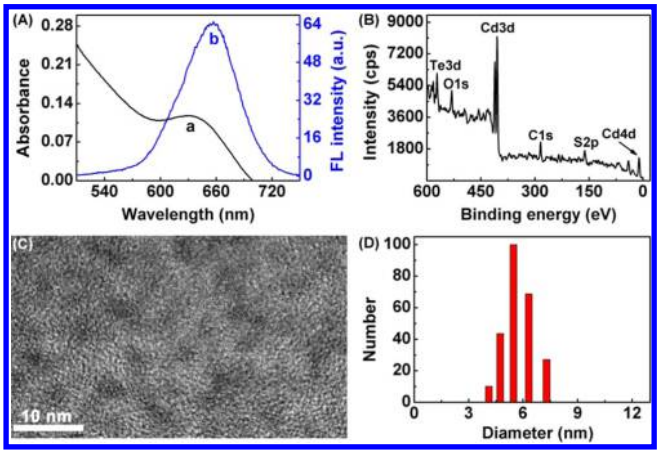

Figure 1. (A) UV−vis (a) and fluorescence (b) spectra (excitation wavelength: 505 nm), (B) XPS spectrum and (C) TEM image of CdTe QDs. (D) Hydrodynamic sizes of CdTe QDs measured by DLS.

light-harvesting extended to the visible region and providing a mild environment for photoelectrochemical detection. Meanwhile, a strong fluorescent emission peak was observed at 657 nm (Figure 1A, curve b), which was consistent with the inflection point of the absorption spectrum, confirming the band gap emission of the core.[20] In addition, the composition of the QDs was characterized by XPS (Figure 1B). The XPS spectrum exhibited two strong peaks at 404.5 and 572.4 eV, corresponding to the Cd 3d and Te 3d levels of QDs, respectively. Carbon (284.4 eV of C 1s), oxygen (531.8 eV of O 1s), and sulfur (161.1 eV of S 2p) were also observed as a result of surface modification of the MPA. Moreover, the Cd/Te atom ratio was 4:1, confirming most Cd atoms at the QDs' surfaces were stabilized by thiol ligands instead of Te atoms and prevented from the oxidation of Te.[37]

dx.doi.org/10.1021/ac503741x | Anal. Chem. 2014, 86, 12362−12368

To characterize the morphology of CdTe QDs, a TEM image and DLS spectrum of the QDs were obtained. As displayed in Figure 1C, the CdTe QDs were distributed uniformity and exhibited a regular spherical structure, with an average size of 4.5 nm. Moreover, the mean hydrodynamic diameter of CdTe QDs was 5.7 nm (Figure 1D), which was consistent with the results of the TEM image.

Feasibility of Photoelectrochemical Biosensor. To test the feasibility and stepwise fabrication of the photoelectrochemical biosensor, CD spectra of different DNAs were recorded (Figure 2A). Different from the C-DNA (curve a) and label-free DNA probe (curve b), their mixture showed a large negative band around 210 nm after incubation for 1 h, suggesting the formation of THMB (curve c).[38,39] Upon addition of target DNA, the characteristic band of THMB at 210 nm was reduced in magnitude while the negative band at 246 nm was increased dramatically in magnitude, indicating the unfolding of THMB and the formation of a B-form DNA duplex (curve d).[40]

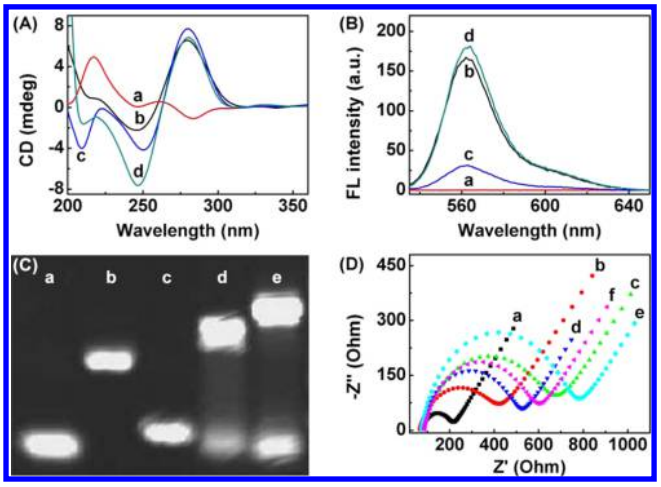

Figure 2. (A) CD spectra of 10 μM C-DNA (a), 10 μM label-free DNA probe (b), THMB (c), and mixture c + 10 μM target DNA (d) in pH 5.3 PBS. (B) Fluorescence spectra of 1.0 μM C-DNA (a), 1.2 μM dual-labeled DNA probe (b), mixture b + 1 μM C-DNA (c), and mixture c + 1.0 μM target DNA (d) in pH 5.3 PBS. Excitation wavelength: 540 nm. (C) PAGE analysis of C-DNA (a), label-free DNA probe (b), target DNA (c), C-DNA + label-free DNA probe (d), and THMB + target DNA (e). (D) EIS spectra of bare ITO (a), CdTe (b), CdTe/C-DNA (c), mixture c blocked by MEA (d), and CdTe/hemin-labeled THMB (e) modified ITO electrode, and mixture e hybridized with target DNA (f) in 0.1 M Na_2SO_4 solution containing a 5 mM $K_4[Fe(CN)_6]/K_3[Fe(CN)_6]$ (1:1) mixture.

To further verify the successful formation and dissociation of THMB in the triplex DNA-based system (Figure 2B), a double-labeled DNA probe with BHQ2 at the 3′ terminus and Cy3 at the 5′ terminus was designed. As expected, no fluorescent signal for C-DNA (curve a) and a strong signal for double-labeled DNA probe (curve b) were observed. After hybridization of C-DNA with the DNA probe (curve c) for 1 h, THMB was formed and led to the quenching of fluorescence. When the target DNA was added, the fluorescence intensity recovered dramatically because the formation of duplex DNA separated the BHQ2 and Cy3 (curve d), which was essentially in agreement with the CD results. Moreover, the hybridization and subsequent opening of THMB were also verified by PAGE analysis (Figure 2C). When the mixture contained C-DNA (lane a) and the DNA probe (lane b), a new band was observed at a short electrophoresis distance, whereas the bands of the C-DNA and DNA probe were pale, which could be attributed to the formation of THMB (lane d). After adding the target DNA (lane c) to the as-prepared THMB sample, a band at a shorter electrophoresis distance was obtained (lane e), and the band of the C-DNA became bright again, indicating the successful recognition of the DNA probe to target DNA and then the release of the C-DNA.

The stepwise assembly process of the biosensor was further studied by EIS (Figure 2D). When CdTe was coated onto the ITO surface, the impedance spectrum of the CdTe-modified ITO electrode (curve b) exhibited a higher charge-transfer resistance (R_{ct}) compared with the ITO electrode (curve a). With the C-DNA (curve c) assembled, the value of R_{ct} increased significantly. After being blocked with MEA (curve d), the R_{ct} value declined as a result of the electrostatic interaction between the positively charged MEA and the negatively charged probe. Moreover, the R_{ct} value of the CdTe/hemin-labeled THMB-modified ITO electrode increased significantly (curve e) and then decreased again after hybridization with the target DNA (curve f), suggesting the photoelectrochemical sensor was constructed as expected and providing a sensitive sensing platform for DNA detection.

Mechanism of Photoelectrochemical Biosensing. The photoelectrochemical strategy is mainly based on hemin-mediated catalytic decomposition of H_2O_2 for in situ generation of O_2.[35] To verify the validity of the proposed mechanism, we employed PEC and CV methods to investigate the reaction pathway of hemin with H_2O_2. The photoelectrochemical measurements of modified electrodes were recorded in different electrolytes (Figure 3A). In 1.0 mM H_2O_2 N_2-saturated PBS, no photoresponse was observed for the ITO electrode owing to a lack of photoelectrochemically active species (curve a). With the introduction of the CdTe QDs, the photocurrent of the CdTe/C-DNA-modified ITO electrode was enhanced to 33 nA (curve b). However, when the electrolyte was replaced by air-saturated PBS involving ~60 μM O_2, the photocurrent of the CdTe/hemin-labeled THMB-modified ITO electrode increased to 102 nA (curve d), which was 6 times higher than that in N_2-saturated PBS (curve c). These results suggest that O_2 was more sensitive to a photoelectrochemical response than H_2O_2.[41] More interestingly, compared with the CdTe/C-DNA-modified ITO

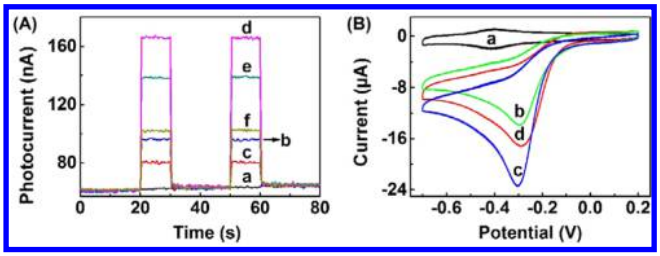

Figure 3. (A) Photocurrent responses of the bare ITO electrode (a), CdTe/C-DNA-modified ITO electrode (b) in N_2-saturated pH 7.4 PBS containing 1.0 mM H_2O_2, CdTe/hemin-labeled THMB-modified ITO electrode in N_2-saturated pH 7.4 PBS (c), air-saturated pH 7.4 PBS (d), mixture c + 1.0 mM H_2O_2 without (e) and with (f) target DNA. (B) Cyclic voltammograms of hemin/glassy carbon electrode in N_2-saturated pH 7.4 PBS (a), mixture a + 0.4 mM H_2O_2 (b), mixture a + 0.8 mM H_2O_2 (c), and air-saturated pH 7.4 PBS (d). Scan rate: 100 mV s^{-1}.

dx.doi.org/10.1021/ac503741x | Anal. Chem. 2014, 86, 12362−12368

electrode (curve b), the photocurrent of the CdTe/hemin-labeled THMB-modified ITO electrode increased to 2.4 times in 1.0 mM H_2O_2 N_2-saturated PBS (curve e). This result suggested that hemin may catalyze the decomposition of H_2O_2 to produce O_2 as an electron acceptor for enhancement of the photocurrent, which could explain the decline of the biosensor in the presence of the target DNA (curve f).

Figure 3B examined the performance of a hemin-modified glassy carbon electrode in different electrolytes using CV measurements in the potential range from −0.7 to 0.2 V. A pair of well-defined redox peaks were observed at −0.41 V in an N_2-saturated atmosphere (curve a), indicating the direct electrochemistry of hemin with the characteristic of one electron transfer process of Fe^{3+}/Fe^{2+}.[42] In the presence of dissolved oxygen, the modified electrode showed a strong cathodic peak at −0.29 V (curve d), attributed to a hemin-facilitated catalytic reduction of O_2. More interestingly, upon addition H_2O_2 to the N_2-saturated PBS buffer, a clear cathodic peak was also observed around −0.29 V, and the current response of the modified electrode was related to the concentration of H_2O_2 in the electrolyte (curves b and c). These results suggested that hemin could catalyze H_2O_2 to form a certain amount of O_2,[43,44] and then the latter was employed as an electron acceptor for enhancement of the photocurrent.

To further investigate the reaction pathway of hemin with H_2O_2, UV spectra were also obtained (Figure 4). First, the

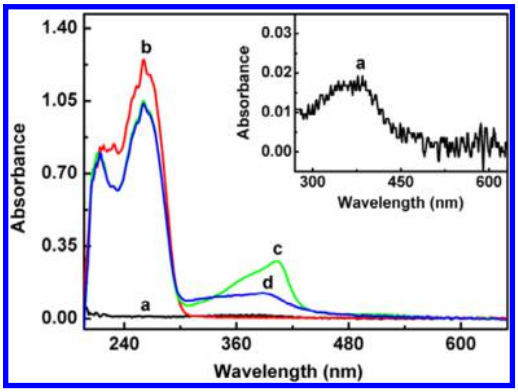

Figure 4. UV−vis spectra of 30 μM hemin (a), 30 μM C-DNA (b), 30 μM HLDP (c), and mixture c +0.6 mM H_2O_2 (d) in pH 7.4 PBS.

spectrum of the hemin showed a weak absorption of the Soret band at 385 nm, indicating the low solubility of hemin (inset in Figure 4, curve a).[45] Different from hemin and C-DNA (curve b), the absorbance band of HLDP exhibited a typical DNA absorption at 260 nm and a clear red shift from 385 to 405 nm (curve c), confirming the successful assembly of hemin with DNA. Meanwhile, the absorption intensity of HLDP increased greatly compared with free hemin, suggesting the hemin species decorated by DNA was active monomers. However, after adding H_2O_2 solution, hemin's Soret band decreased again and blue-shifted from 405 to 388 nm (curve d), revealing hemin was rapidly oxidized to form the highly radical cation hemin[Fe(IV)═$O^{\bullet+}$] and then decayed via some possible pathways.[46,47] Thus, a probable pathway of catalytic reaction might be described below:[48−50]

$$\text{hemin[Fe(III)]} + H_2O_2 \rightarrow \text{hemin[Fe(IV)}{=}O^{\bullet+}\text{]} + H_2O \quad (1)$$

$$\text{hemin[Fe(IV)}{=}O^{\bullet+}\text{]} + H_2O_2 \rightarrow \text{hemin[Fe(III)]} + H_2O + O_2 \quad (2)$$

When H_2O_2 was added, it could oxidize hemin to the highly radical cation (eq 1), which was a transient species and immediately decayed via eq 2. During this process, O_2 was generated, leading to the increase in the photoelectrochemical response. Thus, a hemin-labeled DNA probe can serve as an efficient signal tag and specific recognition module for photoelectrochemical biosensing.

Optimization of Detection Conditions. To achieve excellent photoelectrochemical performance in a sensitive assay of DNA, several experimental parameters, such as H_2O_2 concentration, capture DNA concentration, and the hybridization and dehybridization time of hemin-labeled THMB, were optimized (Figure 5). Because the electrolyte concentration has

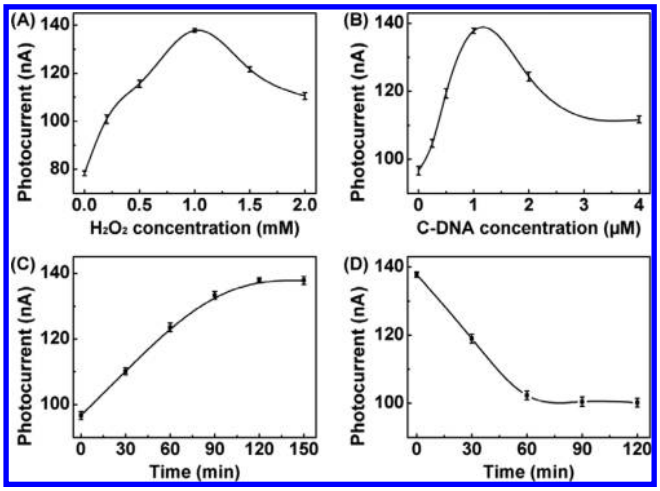

Figure 5. Effects of (A) H_2O_2 concentration, (B) C-DNA concentration, (C) hybridization, and (D) dehybridization time of hemin-labeled THMB on photocurrent responses of the biosensor. When one parameter changes, the others are under their optimal conditions.

a significant influence on the performance of sensing system, the photocurrent was measured at different H_2O_2 concentrations (Figure 5A). The photocurrent was enhanced with a H_2O_2 concentration up to 1.0 mM and then gradually decreased with further addition of H_2O_2, attributed to the surface oxidation of CdTe QDs caused by excess H_2O_2.[51] Thus, 1.0 mM of H_2O_2 was selected as the optimal concentration.

Moreover, the surface density of C-DNA immobilized on a modified electrode greatly affected the sensitivity of photoelectrochemical performance (Figure 5B).[52] When the C-DNA concentration was increased, the photocurrent increased correspondingly in the range of 0−1.0 μM and gradually declined with further addition of C-DNA, indicating a high surface density of C-DNA could decrease the DNA hybridization efficiency, resulting from steric crowding.[53] Therefore, 1.0 μM was selected for the next experiments.

Similarly, the performance of the photoelectrochemical biosensor was also dependent on the THMB's formation and unfolding. As shown in Figure 5C, when the self-assembly time was increased, the photocurrent intensity was enhanced and then tended to a plateau after 120 min, suggesting the hybridization reaction nearly reached the maximum. Thus, 120 min was employed for the optimal time of THMB formation.

dx.doi.org/10.1021/ac503741x | Anal. Chem. 2014, 86, 12362−12368

Furthermore, Figure 5D displays the effect of the incubation time of the target and hemin-labeled THMB on the photocurrent response. When the incubation time was more than 60 min, no desirable photocurrent change was observed, indicating this time was sufficient for target hybridization, so 60 min was selected as the optimal reaction time.

Analytical Performance of Photoelectrochemical Biosensor. On the basis of the hemin-mediated catalytic reaction and target-induced structure switching, the photoelectrochemical biosensor was applied for sensitive detection of DNA. Figure 6A shows the photoelectrochemical signals

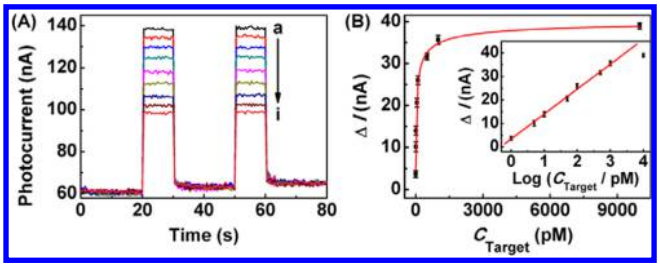

Figure 6. (A) Photocurrent responses of the biosensor at 0, 1, 5, 10, 50, 100, 500, 1000, and 10 000 pM target DNA (from a to i). (B) Plot of photocurrent change vs target DNA concentration. Inset: calibration curve.

measured at various concentrations of DNA. In the absence of target DNA, a high photocurrent was obtained as a result of the generation of oxygen resulting from the hemin-mediated catalytic reaction toward H_2O_2. As the concentration of the DNA increased, the photocurrent intensity decreased gradually, indicating that the dehybridization of THMB released hemin-labeled DNA and then decreased the production of oxygen.

The calibration plot displayed a good linear relationship between ΔI ($\Delta I = I_0 - I$) and the logarithm of the target DNA concentration in a range of 1−1000 pM, where I_0 and I were the photocurrents of the biosensor before and after hybridization with the target DNA (inset in Figure 6B). The linear range is wider than that of the hemin/G-quadruplex-stimulated photoelectrochemical detection method (2−100 nM).[22] The regression equation was ΔI (nA) = 3.43 + 10.61 log C (pM) with a correlation coefficient of 0.997. The detection limit was estimated to be 0.8 pM at 3σ, which was much lower than the 0.2 nM of the DNA-linked hemin/graphene oxide-based fluorescence DNA biosensor[31] and 2.5 pM of the G-quadruplex-based isothermal exponential amplification for DNA colorimetric detection.[54] Obviously, the excellent analytical performance of this proposed sensor was ascribed to the high catalytic activity of DNA-linked hemin.

To investigate the selectivity of the designed biosensor, the effect of different DNA sequences, such as target DNA, smDNA, and tmDNA, on the photocurrent changes was examined (Figure 7). The ΔI of complete complementary target DNA was 4.3- and 6.7-fold higher than that of smDNA and tmDNA, respectively. These results indicated the biosensor had excellent selectivity for target DNA against base mismatched sequences. Moreover, the biosensor of DNA exhibited acceptable precision and reproducibility, with a relative standard deviation of 3.0% for five independent electrodes. Meanwhile, the photocurrent intensity of the biosensor had no obvious change after storage for 10 days, showing good long-time stability.

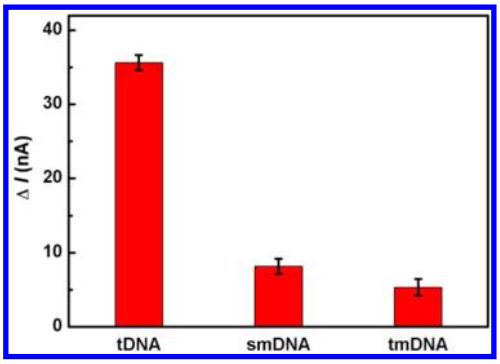

Figure 7. Photocurrent changes of the designed biosensor at 1 nM target DNA, smDNA, and tmDNA.

CONCLUSION

The novel photoelectrochemical sensing strategy was constructed by in situ generation of an electron acceptor via the catalytic reaction of hemin for DNA detection. The hemin-labeled triple-helix molecular beacon structure was first designed, in which hemin showed highly efficient catalytic activity as a result of good water solubility and few inactive dimers. With the catalytic reaction of hemin toward H_2O_2, O_2 as an electron acceptor was generated and subsequently facilitated the substantial enhancement of the photoelectrochemical response. The photoelectrochemical mechanism was also identified to be based on that O_2 is a more effective electron acceptor than H_2O_2. Coupling THMB structure switching with in situ generation of O_2 as a coreactant, a photoelectrochemical biosensor for detection of DNA with high sensitivity, wide linear range, and excellent selectivity has been achieved. Because other biomimetic materials can catalyze decomposition of H_2O_2 to O_2, this designed strategy provides a universal tool for construction of photoelectrochemical devices in bioanalysis.

AUTHOR INFORMATION

Corresponding Author

*Phone/Fax: +86-25-83593593. E-mail: jpl@nju.edu.cn.

Notes

The authors declare no competing financial interest.

ACKNOWLEDGMENTS

We gratefully acknowledge the National Basic Research Program (2010CB732400) and National Natural Science Foundation of China (21375060, 21135002, 21121091).

REFERENCES

(1) Furst, A.; Landefeld, S.; Hill, M. G.; Barton, J. K. *J. Am. Chem. Soc.* **2013**, *135*, 19099−19102.
(2) Lockhart, D. J.; Winzeler, E. A. *Nature* **2000**, *405*, 827−836.
(3) Cai, Z. M.; Chen, Y. Y.; Lin, C. S.; Wu, Y. F.; Yang, C. J.; Wang, Y. R.; Chen, X. *Biosens. Bioelectron.* **2014**, *61*, 370−373.
(4) Grossmann, T. N.; Röglin, L.; Seitz, O. *Angew. Chem., Int. Ed.* **2007**, *46*, 5223−5225.
(5) Gao, Y.; Li, B. X. *Anal. Chem.* **2013**, *85*, 11494−11500.
(6) Lu, C. H.; Wang, F. A.; Willner, I. *J. Am. Chem. Soc.* **2012**, *134*, 10651−10658.
(7) Xia, F.; White, R. J.; Zuo, X. L.; Patterson, A.; Xiao, Y.; Kang, D.; Gong, X.; Plaxco, K. W.; Heeger, A. J. *J. Am. Chem. Soc.* **2010**, *132*, 14346−14348.

(8) Zheng, J.; Jiao, A. L.; Yang, R. H.; Li, H. M.; Li, J. S.; Shi, M. L.; Ma, C.; Jiang, Y.; Deng, L.; Tan, W. H. *J. Am. Chem. Soc.* **2012**, *134*, 19957−19960.
(9) Hu, R.; Liu, T.; Zhang, X. B.; Huan, S. Y.; Wu, C. C.; Fu, T.; Tan, W. H. *Anal. Chem.* **2014**, *86*, 5009−5016.
(10) Baeissa, A.; Dave, N.; Smith, B. D.; Liu, J. W. *ACS Appl. Mater. Interfaces* **2010**, *2*, 3594−3600.
(11) Kong, R. M.; Song, Z. L.; Meng, H. M.; Zhang, X. B.; Shen, G. L.; Yu, R. Q. *Biosens. Bioelectron.* **2014**, *54*, 442−447.
(12) Liu, S. L.; Li, C.; Cheng, J.; Zhou, Y. X. *Anal. Chem.* **2006**, *78*, 4722−4726.
(13) Tang, X. F.; Zhao, D.; He, J. C.; Li, F. W.; Peng, J. X.; Zhang, M. N. *Anal. Chem.* **2013**, *85*, 1711−1718.
(14) Grätzel, M. *Nature* **2001**, *414*, 338−344.
(15) Chen, D.; Zhang, H.; Li, X.; Li, J. H. *Anal. Chem.* **2010**, *82*, 2253−2261.
(16) Long, Y. T.; Kong, C.; Li, D. W.; Li, Y.; Chowdhury, S.; Tian, H. *Small* **2011**, *7*, 1624−1628.
(17) Zeng, X. X.; Ma, S. S.; Bao, J. C.; Tu, W. W.; Dai, Z. H. *Anal. Chem.* **2013**, *85*, 11720−11724.
(18) Haddour, N.; Chauvin, J.; Gondran, C.; Cosnier, S. *J. Am. Chem. Soc.* **2006**, *128*, 9693−9698.
(19) Zhang, X. R.; Xu, Y. P.; Yang, Y. Q.; Jin, X.; Ye, S. J.; Zhang, S. S.; Jiang, L. L. *Chem.—Eur. J.* **2012**, *18*, 16411−16418.
(20) Wang, W. J.; Bao, L.; Lei, J. P.; Tu, W. W.; Ju, H. X. *Anal. Chim. Acta* **2012**, *744*, 33−38.
(21) Wang, M.; Yin, H. S.; Shen, N. N.; Xu, Z. N.; Sun, B.; Ai, S. Y. *Biosens. Bioelectron.* **2014**, *53*, 232−237.
(22) Golub, E.; Niazov, A.; Freeman, R.; Zatsepin, M.; Willner, I. *J. Phys. Chem. C* **2012**, *116*, 13827−13834.
(23) Wu, Y. P.; Zhang, B. T.; Guo, L. H. *Anal. Chem.* **2013**, *85*, 6908−6914.
(24) Tanne, J.; Schäfer, D.; Khalid, W.; Parak, W. J.; Lisdat, F. *Anal. Chem.* **2011**, *83*, 7778−7785.
(25) Zhao, W. W.; Ma, Z. Y.; Yan, D. Y.; Xu, J. J.; Chen, H. Y. *Anal. Chem.* **2012**, *84*, 10518−10521.
(26) Song, Y. J.; Qu, K. G.; Zhao, C.; Ren, J. S.; Qu, X. G. *Adv. Mater.* **2010**, *22*, 2206−2210.
(27) Deng, S. Y.; Lei, J. P.; Huang, Y.; Cheng, Y.; Ju, H. X. *Anal. Chem.* **2013**, *85*, 5390−5396.
(28) Xue, T.; Jiang, S.; Qu, Y. Q.; Su, Q.; Cheng, R.; Dubin, S.; Chiu, C. Y.; Kaner, R.; Huang, Y.; Duan, X. F. *Angew. Chem., Int. Ed.* **2012**, *51*, 3822−3825.
(29) Genfa, Z.; Dasgupta, P. K. *Anal. Chem.* **1992**, *64*, 517−522.
(30) Bruice, T. C. *Acc. Chem. Res.* **1991**, *24*, 243−249.
(31) Wang, Q. B.; Xu, N.; Lei, J. P.; Ju, H. X. *Chem. Commun.* **2014**, *50*, 6714−6717.
(32) Golub, E.; Freeman, R.; Willner, I. *Angew. Chem., Int. Ed.* **2011**, *50*, 11710−11714.
(33) Stefan, L.; Denat, F.; Monchaud, D. *J. Am. Chem. Soc.* **2011**, *133*, 20405−20415.
(34) Freeman, R.; Liu, X. Q.; Willner, I. *J. Am. Chem. Soc.* **2011**, *133*, 11597−11604.
(35) Zhang, J. J.; Wang, W. T.; Chen, S. H.; Ruo, Y.; Zhong, X.; Wu, X. P. *Biosens. Bioelectron.* **2014**, *57*, 71−76.
(36) Mak, J. S. W.; Farah, A. A.; Chen, F. F.; Helmy, A. S. *ACS Nano* **2011**, *5*, 3823−3830.
(37) Borchert, H.; Talapin, D. V.; Gaponik, N.; McGinley, C.; Adam, S.; Lobo, A.; Möller, T.; Weller, H. *J. Phys. Chem. B* **2003**, *107*, 9662−9668.
(38) Song, Y. J.; Feng, L. Y.; Ren, J. S.; Qu, X. G. *Nucleic Acids Res.* **2011**, *39*, 6835−6843.
(39) Feng, L. Y.; Huang, Z. Z.; Ren, J. S.; Qu, X. G. *Nucleic Acids Res.* **2012**, *40*, e122.
(40) Vorlíčková, M.; Kejnovská, I.; Bednářová, K.; Renčiuk, D.; Kypr, J. *Chirality* **2012**, *24*, 691−698.
(41) Zhang, X. R.; Liu, M. S.; Liu, H. X.; Zhang, S. S. *Biosens. Bioelectron.* **2014**, *56*, 307−312.
(42) Guo, Y. J.; Deng, L.; Li, J.; Guo, S. J.; Wang, E. K.; Dong, S. J. *ACS Nano* **2011**, *5*, 1282−1290.
(43) Yang, Q. L.; Nie, Y. J.; Zhu, X. L.; Liu, X. J.; Li, G. X. *Electrochim. Acta* **2009**, *55*, 276−280.
(44) Wang, B. Z.; Anzai, J.; Gong, W. L.; Wang, M. Q.; Du, X. Y. *Sens. Mater.* **2008**, *20*, 221−230.
(45) Jiang, X. Y.; Chai, Y. Q.; Wang, H. J.; Yuan, R. *Biosens. Bioelectron.* **2014**, *54*, 20−26.
(46) Onuoha, A. C.; Zu, X. L.; Rusling, J. F. *J. Am. Chem. Soc.* **1997**, *119*, 3979−3986.
(47) Stefan, L.; Denat, F.; Monchaud, D. *Nucleic Acids Res.* **2012**, *40*, 8759−8772.
(48) Lu, X. B.; Zhou, J. H.; Lu, W.; Liu, Q.; Li, J. H. *Biosens. Bioelectron.* **2008**, *23*, 1236−1243.
(49) Tang, Y. J.; Guo, Y. J.; Zhang, L.; Cai, J. Y.; Yang, P. H. *Biosens. Bioelectron.* **2014**, *54*, 628−633.
(50) Xuan, J.; Jia, X. D.; Jiang, L. P.; Abdel-Halim, E. S.; Zhu, J. J. *Bioelectrochemistry* **2012**, *84*, 32−37.
(51) Mancini, M. C.; Kairdolf, B. A.; Smith, A. M.; Nie, S. M. *J. Am. Chem. Soc.* **2008**, *130*, 10836−10837.
(52) Southern, E.; Mir, K.; Shchepinov, M. *Nat. Genet.* **1999**, *21*, 5−9.
(53) Zhang, J.; Song, S. P.; Zhang, L. Y.; Wang, L. H.; Wu, H. P.; Pan, D.; Fan, C. H. *J. Am. Chem. Soc.* **2006**, *128*, 8575−8580.
(54) Nie, J.; Zhang, D. W.; Tie, C.; Zhou, Y. L.; Zhang, X. X. *Biosens. Bioelectron.* **2014**, *56*, 237−242.